1
2
3 **Characterization of enterovirus D68 infection in four nonhuman primate species**
4
5

6 Justin Dearing[1], Abigail Conte[2], Catherine Brooks[1], Anna Zimina[3], Rhiannon Rivas[1], Sharla M.
7 Birch[1], Danielle R. Adney[1], Maggie Li[2], Adriana Rascon[1], George A. Belov[3], Andrew Pekosz[2] and
8 Meghan S. Vermillion[1]
9
10
11 [1]Department of Comparative Medicine, Lovelace Biomedical Research Institute, Albuquerque,
12 NM, USA
13 [2]W. Harry Feinstone Department of Molecular Microbiology and Immunology, The Johns Hopkins
14 Bloomberg School of Public Health, Baltimore, MD, USA
15 [3]Department of Veterinary Medicine, University of Maryland, and VA-MD College of Veterinary
16 Medicine, College Park, MD 20742, USA
17
18
19
20
21 **Correspondence:** Meghan S. Vermillion
22 Department of Comparative Medicine
23 Lovelace Biomedical Research Institute
24 2425 Ridgecrest Drive SE
25 Albuquerque, NM 87108
26 E: mvermillion@lovelacebiomedical.org
27 P: 505-717-3242
28
29

30 **Disclosure:** The authors report no conflicts of interest in this work.
31
32 **Abbreviated title:** EV-D68 in Nonhuman Primates
33
34 **Key words:** EV-D68, non-polio enterovirus, respiratory enterovirus, acute flaccid myelitis, AFM,
35 NHP, macaque, monkey

Abstract

Human enterovirus D68 (EV-D68) is a globally reemerging respiratory pathogen that is associated with the development of acute flaccid myelitis (AFM) in children. Currently, there are no approved vaccines or treatments for EV-D68 infection, and there is a paucity of data related to the virus and host specific factors that predict disease severity and progression to the neurologic syndrome. Published animal models of EV-D68 infection to date have been limited to mice, cotton rat and ferrets, and investigation of the susceptibility of nonhuman primate (NHP) species to contemporary EV-D68 isolates has not yet been reported. In this study, we challenged juvenile NHPs – cynomolgus macaques, rhesus macaques, pigtailed macaques, and African green monkeys – with one of five different 2014 or 2018 EV-D68 isolates by the respiratory route. Animals were monitored for clinical respiratory and neurologic signs, and serially collected nasal swabs, bronchoalveolar lavage fluid (BALF) and cerebrospinal fluid (CSF) were evaluated for EV-D68 RNA and infectious virus. Infection with 2014 and 2018 EV-D68 isolates resulted in mild respiratory and gastrointestinal disease in some animals, but no evidence of neurological disease. Neither EV-D68 RNA nor infectious virus could be detected from any sample collected from animals challenged with 2014 EV-D68 isolates. Limited viral shedding – based on viral RNA quantified from nasal swabs and BALF – was detected from some animals infected with 2018 EV-D68 isolates. No virus was detectable in CSF. The rate of seroconversion was 100% for cynomolgus macaques infected with the 2018 EV-D68 isolates, but averaged between 0-50% for the 2014 isolates. Based on the results of this study, there is some evidence that infection with 2018 EV-D68 isolates may be more reliable at establishing limited infection than 2014

59   EV-D68 isolates. Regardless of virus isolate, however, EV-D68 infection of juvenile NHP

60   species resulted in mild and nonspecific clinical disease and limited viral shedding. These

61   data suggest that further refinements to the NHP model system (e.g., immunosuppression

62   and/or direct viral inoculation) may be required to reproduce EV-D68 infection of the

63   central nervous system and the associated AFM phenotype.

Introduction

Human enterovirus D68 (EV-D68) is a non-polio enterovirus that can cause severe respiratory illness, and infection has been linked with a neurologic syndrome known as acute flaccid myelitis (AFM), which is most commonly reported in children (Lang et al., 2014). Over the past two decades, the incidence of reported EV-D68 infections has continued to increase worldwide, and periods of heightened detection have coincided with biennial outbreaks of AFM (Chong et al., 2018; Dyda et al., 2018; Greninger et al., 2015; Kamau et al., 2019; Knoester et al., 2019; Messacar et al., 2016). At present, there are no approved vaccines or therapies for EV-D68 infection, and the existing treatments for AFM patients are non-specific and largely anecdotal. Development and testing of more targeted EV-D68 vaccines and therapies relies on a comprehensive understanding of EV-D68 pathogenesis *in vivo,* including cell receptor usage, mechanisms of viral dissemination and tissue tropisms, as well as host innate and adaptive immune responses.

Experimental EV-D68 infection has been described in mice, cotton rats, and ferrets. Productive infection of mice with either historic or contemporary EV-D68 isolates requires inoculation into either neonates or immunocompromised adults (Hixon, Yu, et al., 2017; Hurst et al., 2019; Morrey et al., 2018; Zhang, Zhang, Dai, et al., 2018). With each of these mouse models, the incidence and onset of AFM following infection is based on EV-D68 isolate and route of infection. Studies using these mouse models have been instrumental in demonstrating the increased virulence of contemporary versus historic EV-D68 isolates, and have served as platforms for demonstrating efficacy of candidate vaccines and antiviral treatments (Evans et al., 2019; Hixon, Clarke, et al., 2017; Vogt et

87   al., 2020; Zhang, Zhang, Zhang, et al., 2018; Zheng et al., 2018). In a single published

88   report, ferrets were shown to be permissive to the prototype EV-D68 Fermon strain, but

89   respiratory infection did not result in significant respiratory illness, nor any evidence of

90   AFM symptoms (Zheng et al., 2017). Similar to EV-D68 infection in ferrets, infection of

91   cotton rats with either EV-D68 Fermon, EV-D68 VANBT/1 (pre-outbreak isolate) or EV-

92   D68 MO/14/19 (outbreak isolate) revealed productive respiratory infection without any

93   signs of AFM symptoms. Moreover, viral replication in the cotton rat is reported to be very

94   rapid, with peak viral titers detected at 10 hours post-infection and viral clearance by 48

95   hours post-infection (Patel et al., 2016).

96   Nonhuman primates (NHPs) are the most phylogenetically similar preclinical

97   species to humans, and as such, represent the gold standard for modelling human

98   physiology and pathology, and for predicting human pharmacologic and toxicologic

99   responses to candidate therapeutic compounds. The relatively large size of NHPs as

100   compared with rodent models provides the additional advantage of increased sample

101   collection volumes and frequencies, as well as the feasibility of collecting additional types

102   of samples that mirror clinical sampling protocols. For example, viral challenge studies in

103   nonhuman primates permit serial sampling of various biological compartments (e.g.,

104   bronchoalveolar lavage fluid) to characterize viral replication kinetics in sample types with

105   direct clinical relevance (Vermillion et al., 2021). Moreover, advanced imaging techniques

106   (e.g., MRI) and electromyography protocols are established for NHPs, providing

107   additional translational utility for localizing spinal cord lesions and characterizing the

108   patterns of denervation associated with AFM that can be correlated with human clinical

109   cases.

110   Relevant to EV-D68, NHPs have been shown to harbor many different simian

111   enteroviruses, with up to 72% amino acid identity to related human enteroviruses (Nix et

112   al., 2008). Further, NHPs have been instrumental in the study of poliovirus infection and

113   associated disease, as both rhesus and cynomolgus macaques have been shown to be

114   susceptible to poliovirus infection and associated poliomyelitis following oral viral

115   inoculation (Shen et al., 2017). Experimental infection of NHPs with EV-D68 is limited to

116   a study in rhesus macaques, in which intranasal infection with EV-D68 (Kunming Strain)

117   resulted in detectable virus in serially collected nasal swabs, blood, and fecal specimens

118   out to 14 days post-infection (Zheng et al., 2018). Rhesus macaques have also been

119   shown to mount potent neutralizing responses following immunization with an inactivated

120   EV-D68 vaccine (Zheng et al., 2020). The susceptibility of other nonhuman primate

121   species to EV-D68 infection and comparisons of nonhuman primate susceptibility to

122   contemporary EV-D68 isolates, however, has not yet been evaluated.

123   In this study, juvenile NHPs – cynomolgus macaques, rhesus macaques, pigtailed

124   macaques, and African green monkeys – were inoculated intratracheally and intranasally

125   with one of five different 2014 or 2018 EV-D68 isolates (US/MO/2014-18947, US/IL/2014-

126   18952, US/MD/2018-23209, US/MN/2018-23263, and US/WA/2018-23201) (**Table 1**).

127   We report the results of clinical respiratory and neurologic monitoring, viral detection in

128   nasal swabs, bronchoalveolar lavage and cerebrospinal fluid, and histopathology of

129   respiratory and central nervous system tissues (**Fig. 1**). These collective data provide the

130   first characterization of EV-D68 infection in NHP model systems.

Results

EV-D68 infection resulted in mild and sporadic clinical disease in all NHP species.

Following EV-D68 infection, animals were monitored daily for clinical respiratory, gastrointestinal and neurological abnormalities. Body weights were obtained concurrent with anesthetized sample collection procedures. For all animals, regardless of the EV-D68 strain, clinical observations were limited to mild gastrointestinal and respiratory signs, and no neurologic abnormalities were observed from any animal during the observation period in this study (**Table 2**). For animals infected with the 2014 EV-D68 isolates, the majority of clinical observations were made 8 days post-infection (dpi) or later, and abnormal feces (i.e., soft stool or diarrhea) were the most commonly reported clinical sign (**Fig. 2a**), and nasal and/or ocular discharge was reported sporadically (**Fig. 2b**). Compared with cynomolgus macaques and pigtailed macaques, African green monkeys infected with either 2014 EV-D68 isolate had fewer clinical signs reported. There were no obvious differences in disease incidence or character when comparing infection with the IL/2014 and MO/2014 EV-D68 isolates in any NHP species (**Fig. 2a** and **b**). For animals infected with the 2018 EV-D68 isolates, respiratory symptoms were absent over the observation period for this study (**Fig. 2b**). Gastrointestinal symptoms were reported commonly in cynomolgus macaques, but these observations were also made at baseline, which suggests that they were unrelated to the EV-D68 infection (**Fig. 2a**). For both the 2014 and 2018 EV-D68 isolates, evidence of paresis, paralysis, or other neurologic disease was absent in all animals.

153   For all infection groups, average change in body weight over the course of the

154   study was less than 5% of baseline for most animals. Mild body weight loss was observed

155   in some animals during the first week of the study, but was not consistently reported.

156   Overall, animals gained weight over the course of the study, and the average increase in

157   body weight was consistent with published growth curves for juvenile NHPs (Haertel et

158   al., 2018). There was no obvious impact of either NHP species or EV-D68 isolate on body

159   weight changes observed in this study (**Fig. 3a-d**). The absence of uninfected control

160   animals in this study, however, precludes differentiation of any body weight loss or gain

161   that may have been associated with collection procedures or normal expected growth,

162   respectively.

163

164   **EV-D68 infection resulted in limited and transient detection of viral RNA in the**

165   **upper and lower respiratory tract.**

166   In order to assess viral load and viral replication kinetics in the respiratory tract and

167   central nervous system, bronchoalveolar lavage fluid (BALF), nasal swabs, and

168   cerebrospinal fluid (CSF) were serially collected following EV-D68 inoculation (**Fig. 1**).

169   Viral RNA was measured by RT-PCR and infectious virus was detected by median tissue

170   culture infectious dose (TCID$_{50}$) assay. In animals infected with the 2014 EV-D68 isolates,

171   neither viral RNA nor infectious virus could be quantified in any of the samples analyzed

172   (**Table 3**). In animals infected with the 2018 EV-D68 isolates, viral RNA was variably

173   detected within nasal swabs and BALF supernatant collected between 1-5 dpi (**Fig. 4**). In

174   nasal swabs collected 1 dpi, average EV-D68 RNA was quantified between 10^4-10^6

175   copies per swab for each virus isolate, and RNA load in nasal swabs was similar between

rhesus (**Fig. 4a**) and cynomolgus (**Fig. 4c**) macaques. By 3 dpi, viral RNA was below the limit of quantification in nasal swabs collected from all animals except one rhesus macaque challenged with EV-D68 MD/2018 (**Fig. 4a** and **c**). In BALF collected 3 dpi, viral RNA was detectable in one rhesus from each the MD/2018 and WA/2018 infection groups (**Fig. 4b**), and from one cynomolgus macaque from the MN/2018 infection group (**Fig. 4d**). All BALF samples collected 7 dpi were below the assay limit of quantification (**Fig. 4b** and **d**). EV-D68 RNA was not detectable in CSF collected 3 dpi (**Table 3**). All samples evaluated by PCR for viral RNA were also tested for the presence of infectious virus but no infectious virus was detected (data not shown).

Because EV-D68 RNA was only transiently detected in upper and lower respiratory tract samples, western blot for anti-EV-D68 antibodies was performed on serum collected at baseline and at 26 dpi in order to confirm infection (**Fig. 5a**). Other than animal #20-413 (cynomolgus macaque from the MD/2018 infection group), for which baseline antibody screening was inconclusive (data not shown), all baseline serum samples were negative for anti-EV-D68 antibodies, confirming no pre-existing immunity to EV-D68 (**Table 3**). Overall, infection with the 2018 EV-D68 isolates resulted in the greatest seroconversion rate, with 100% of the cynomolgus macaques and between 33-50% of the rhesus macaques having detectable EV-D68 antibodies. Seroconversion for the 2014 EV-D68 isolates was overall lower, ranging from 0-50%. Notably, there was no evidence of seroconversion in African green monkeys infected with either 2014 EV-D68 isolate (**Fig. 5b**).

Interestingly, the presence of anti-EV-D68 antibodies did not always correlate with the presence of detectable EV-D68 RNA in respiratory samples; there were 4 animals (3

199   cynomolgus macaques and 1 pigtailed macaque) with detectable antibodies at 26 dpi that

200   had no detectable virus in either nasal swabs or BALF (**Table 3**). This suggests that there

201   was productive EV-D68 infection that was either not captured within the sampling window

202   or was below the limit of detection of the PCR assay. Surprisingly, there were also 4

203   animals (all rhesus macaques) with detectable EV-D68 RNA in nasal swabs collected 1

204   dpi, but no evidence of serum antibodies at 26 dpi (**Table 3**). It is possible that viral RNA

205   detected in the nasal cavity 1 dpi may represent residual RNA from the EV-D68 inoculum;

206   animal #2002, however, also had detectable viral RNA in nasal swabs collected 3 and 5

207   dpi, which makes this hypothesis less likely. This disparity may also be explained by

208   species-specific differences in immune response to EV-D68 infection.

209

210   **EV-D68 infection resulted in mild airway inflammation without evidence of virus-**

211   **induced pulmonary histopathology.**

212   In order to characterize the airway inflammation following EV-D68 infection, BALF

213   cell pellets were processed and analyzed for total cell counts and cell differentials at each

214   collection timepoint (**Fig. 1**). Due to species-specific variability in the baseline total cell

215   counts in BALF, data were normalized and presented as a percent change from baseline

216   for each post-infection timepoint (**Fig. 6**). Compared with macaques (**Fig. 6a-c**), AGM

217   demonstrated greater overall increases in airway inflammation post-infection, regardless

218   of EV-D68 isolate, though response was highly variable (**Fig. 6d**). This inflammatory

219   response was observed independent of any evidence of EV-D68 infection, based on

220   absence of serum antibodies, suggesting that this response may represent non-specific

221   inflammation related to the BALF collection procedures. Differentiation of procedural-

222   related changes cannot be made without an uninfected control group for comparison.

223   Comparing infection of different EV-D68 isolates within NHP species, EV-D68 MD/2018

224   resulted in a greater induction of airway inflammation than the other EV-D68 isolates

225   evaluated in both cynomolgus macaques and rhesus macaques at 26 dpi (**Fig. 6a** and

226   **b**). Overall, pigtailed macaques showed the smallest increase in airway inflammatory cells

227   over the course of the study (**Fig. 6c**).

228   At 26-28 dpi, animals were euthanized for terminal tissue collections. Terminal lung

229   weights were obtained and normalized to terminal body weights and brain weight, and

230   ratios were calculated for each animal (**Table 4**). Overall, terminal lung weights ranged

231   from 0.6-0.9% of total body weight, and from 12-22% of total brain weight. Some species-

232   specific differences in lung/body weight and lung/brain weight ratios were observed, but

233   within NHP species, there were no clear differences in lung weight ratios between EV-

234   D68 isolates. The absence of age-matched uninfected controls for each NHP species

235   precludes comparison of post-infection organ weight ratios with normal ranges, though

236   the reported lung to body weight ratios are comparable to published reference intervals

237   for NHPs (Miller et al., 2017), suggesting an absence of any significant pulmonary

238   inflammation or edema in lungs collected 26-28 dpi. Sections of the thoracic trachea, left

239   lungs, tracheobronchial lymph nodes, brain and spinal cord were microscopically

240   examined and assessed for evidence of inflammation and/or injury. No evidence of virus-

241   associated pathology was noted for any of the tissues evaluated in this study (data not

242   shown).

Discussion

While *in vitro* studies have significantly expanded our understanding of the mechanisms of EV-D68 cell entry and replication, confirmation of these concepts *in vivo* has yielded variable results (Hixon, Clarke, et al., 2017). Establishing and characterizing additional large animal models of EV-D68 infection and disease is critical for efficacy and safety evaluations for candidate medical countermeasures. Herein, we describe the results of pilot EV-D68 infection studies in juvenile NHPs, in which viral replication kinetics and clinical disease are characterized over 26-28 days following infection by the respiratory route.

In this study, inoculation with either 2014 or 2018 EV-D68 isolates by both the intranasal and intratracheal routes resulted in sporadic, mild and transient clinical disease that was characterized by gastrointestinal and/or upper respiratory symptoms that were most commonly observed 6-14 days post-infection. While the 2014 EV-D68 isolates resulted in sporadic respiratory signs (i.e., nasal or ocular discharge), infection with the 2018 EV-D68 isolates did not. No neurologic abnormalities were observed in any animal during the observation period in this study. Moreover, no gross or histopathological findings were noted in the respiratory tract or spinal cord that could be attributed to EV-D68 infection. Overall, clinical disease and pathology are not consistent components of this model, and are unlikely to serve as a useful markers of efficacy for evaluating candidate medical countermeasures. This outcome is consistent with observations from experimental infections of immunocompetent cotton rats and ferrets, in which clinical disease is minimal or absent (Patel et al., 2016; Zheng et al., 2017). Although the available surveillance data in humans is insufficient for determining the prevalence of

266   clinically silent EV-D68 infections within the general population, it has been estimated that

267   only 10% of EV-D68 respiratory infections resulting in hospitalization are at risk of

268   developing AFM (Dyda et al., 2018; Morens et al., 2019). The absence of neurologic

269   symptoms in this NHP infection study, therefore, is not an unexpected result based on

270   the total number of animals enrolled.

271   Although the specific receptor(s) for EV-D68 remain unknown, sialic acid has been

272   hypothesized, and studies *in vitro* have demonstrated that prototype EV-D68 and isolates

273   from 2010-2011 bind both α2,6- and α2,3-linked sialic acids (Baggen et al., 2016;

274   Imamura et al., 2014). EV-D68 strains isolated from 2012 and onward, however, have

275   also demonstrated sialic acid-independent binding *in vitro* (Baggen et al., 2016; Liu et al.,

276   2015), suggesting that more contemporary EV-D68 strains may use alternative cell

277   receptors, which may influence tissue tropism and disease. One potential limitation of

278   NHP models of respiratory infection is the differential expression and distribution of sialic

279   acid receptors across different cell types within the upper and lower respiratory tract.

280   Compared with humans, who express both α2,6- and α2,3-linked sialic acid residues in

281   ciliated respiratory epithelial cells, sialic acid expression in NHPs is more limited, and

282   receptors are present only on pulmonary Type II pneumocytes, submucosal goblet cells,

283   and upper respiratory tract ciliated epithelium (Kuchipudi et al., 2021). Additional studies

284   are needed to characterize receptor and co-receptor usage by both historic and

285   contemporary EV-D68 isolates in order to predict how this impacts species-specific

286   susceptibility to infection.

287   Indeed, much of the challenge with modeling the AFM phenotype secondary to a

288   respiratory EV-D68 infection stems from the fact that the incidence of this specific disease

289   sequelae is very low in humans. Likewise, even in the perfect model system, incidence

290   of AFM is predicted to be low, which then obligates enrollment of very large cohorts of

291   animals in order to detect the phenotype in a sufficient number to evaluate outcomes. The

292   obvious workarounds to this dilemma are to artificially increase disease incidence through

293   various manipulations of the host and/or virus. Such strategies have been employed in

294   mouse models of EV-D68 infection, where productive viral replication and overt disease

295   require either direct inoculation of the virus into the central nervous system of neonatal

296   animals or the use of immunodeficient mouse strains. Future EV-D68 infection studies in

297   NHPs should consider concurrent immunosuppression and/or direct intrathecal

298   inoculation of virus in order to enhance infection and disease.

Methods

Study Design

A total of 24 animals were exposed to one of five EV-D68 clinical isolates by combined intranasal and intratracheal instillation. The study was conducted in two phases: Phase I (conducted under Lovelace protocol FY20-131A) evaluated the 2014 EV-D68 isolates in n=12 animals, and Phase II (conducted under Lovelace protocol FY20-131B) evaluated the 2018 EV-D68 isolates in n=12 animals. Within each study phase, animals were divided into two cohorts of n=6/cohort – staggered by one day – with even distribution of each study group across cohorts (**Table 1**). Animals were observed daily following inoculation, and blood, bronchoalveolar lavage fluid (BALF), nasal swabs, and cerebrospinal fluid (CSF) were serially collected for determination of viral replication kinetics (**Fig. 1**). Necropsy and terminal tissue collection was performed 26-28 days post-infection for histopathology.

Viruses

The following EV-D68 isolates were evaluated in this study: US/MO/2014-18947 (Clade B1, GenBank Accession No. KM851225), US/IL/2014-18952 (Clade B2, GenBank Accession No. KM851230), US/MD/2018-23209 (Clade B3, GenBank Accession No. MN246002), US/MN/2018-23263 (Clade B3, GenBank Accession No. MN246026), and US/WA/2018-23201 (Clade B3, GenBank Accession No. MN245994). All virus stocks were sourced from ATCC, and all seed and working stocks for animal studies were generated by the Pekosz Laboratory at Johns Hopkins. Human rhabdomyosarcoma (RD)

322   cells were obtained from the American Type Culture Collection (ATCC) (CCL-136) and

323   cultured in Gibco Dulbecco's Minimal Essential Medium (DMEM) supplemented with 10%

324   fetal bovine serum (FBS), 100 U/mL penicillin, 100 µg/mL streptomycin, 1 mM sodium

325   pyruvate and 2 mM GlutaMAX (Gibco). The cells were grown at 37°C in a humidified

326   environment supplemented to 5% CO2. The initial vial of cells was expanded to obtain 20

327   vials of frozen cells which were confirmed to be mycoplasma free. One vial of this stock

328   was thawed and expanded for use, with one additional stock of 20 frozen cells generated

329   from the first passage after thawing. The cultures were passaged up to 20-25 times before

330   new cells were thawed. Virus was stored at -70°C or below until infections. For IN/IT

331   instillations, virus was thawed, diluted with Dulbecco's Modified Eagle Medium (DMEM),

332   and stored on ice until inoculations. Two aliquots of each inoculum were used for back-

333   titration and confirmation of titer by $TCID_{50}$ assay using RD cells. The inoculation stock

334   titers for US/MO/2014-18947 and US/IL/2014-18952 were 2 x 10^7 $TCID_{50}$/mL, and the

335   inoculation stock titers for US/MD/2018-23209, US/MN/2018-23263, and US/WA/2018-

336   23201 were 2 x 10^6 $TCID_{50}$/mL. The VP gene of each virus stock was sequenced to

337   confirm the isolate designation. All virus infections were performed at 32°C.

338

339   *Animals*

340   All animal studies were conducted at Lovelace Biomedical Research Institute (LBRI,

341   Albuquerque, NM). All infection studies were performed in an animal biosafety level 2

342   (ABSL-2) laboratory. All protocols were reviewed by an Institutional Animal Care and Use

343   Committee (IACUC) at LBRI (IACUC #FY20-131). Research was conducted under an

344   IACUC approved protocol in compliance with the Animal Welfare Act, PHS Policy, and

345   other federal statutes and regulations relating to animals and experiments involving

346   animals. The facilities where this research was conducted are accredited by the

347   Association for Assessment and Accreditation of Laboratory Animal Care, International

348   and strictly adhere to principles stated in the Guide for the Care and Use of Laboratory

349   Animals, National Research Council, 2011 (National Academies Press, Washington, DC).

350   A total of 24 animals were used on this study [8 cynomolgus macaques (3M/5F); 8 rhesus

351   macaques (4M/4F); 4 pigtailed macaques (2M/2F); and 4 African green monkeys

352   (2M/2F)]. Cynomolgus macaques and African green monkeys were sourced from World

353   Wide Primates (Miami, FL); rhesus macaques were sourced from Envigo (Alice, TX); and

354   pigtailed macaques were sourced from the University of Washington National Primate

355   Research Center (Mesa, AZ). Animals were between 8.2 and 11.8 months of age and

356   between 1.1 and 2.5 kg at the time of EV-D68 inoculation (**Table 1**). All animals were

357   quarantined for a minimum of 21 days following arrival at LBRI. All animals were tested

358   and confirmed negative for *Mycobacterium tuberculosis*, simian immunodeficiency virus

359   (SIV), simian T-lymphotropic virus-1 (STLV-1), simian retroviruses 1 and 2 (SRV-1 and

360   SRV-2), and *Macacine herpesvirus* 1 (Herpes B virus). Prior to study start, all animals

361   were examined by a laboratory animal veterinarian, and only healthy animals were placed

362   on study. Animals were socially housed in a climate-controlled room with a fixed light/dark

363   cycle (12-h light/12-h dark). Animals were monitored at least twice daily throughout the

364   study. Commercial monkey chow, treats, and fruit were provided twice daily by trained

365   personnel. Water was available ad libitum.

366

367

368   *Viral Inoculations*

369   Animals were anesthetized with ketamine and xylazine and placed in the prone position

370   for EV-D68 infections by both intranasal and intratracheal instillation. The total inoculation

371   was delivered in 2 mL per animal (1 mL delivered intratracheal and 1 mL delivered

372   intranasal – 0.5 mL per nostril). Virus was thawed on wet ice and diluted immediately prior

373   to infections. For intratracheal instillation, a pediatric bronchoscope (Olympus XP-40) was

374   advanced to the level of the carina. Polyethylene (PE) tubing was advanced through the

375   bronchoscope, and 1 mL virus was instilled through the tubing, followed by 0.5 mL sterile

376   saline and approximately 1 mL air. For intranasal instillation, the viral inoculum was

377   administered drop-wise into each nostril using a calibrated pipette (i.e., 0.5 mL per nostril,

378   1 mL total).

379

380   *Clinical Scoring*

381   Animals were observed at baseline and daily post-infection for evidence of clinical

382   disease, including respiratory illness and paresis/paralysis. Respiratory signs were

383   recorded based on a semi-quantitative scoring system comprised on observations of

384   nasal or ocular discharge, cough, labored breathing, and abnormal posture. Signs of

385   paresis or paralysis were recorded based on the number and severity of affected limbs,

386   using an adapted scoring system (Urbanski et al., 2012). Severity of the paresis/paralysis

387   was recorded on a scale of 0-3 (0 = normal motor function; 1 = mild paresis [e.g., slight

388   favoring of contralateral limb and/or reduced gripping with hands/feet]; 2 = moderate

389   paresis [e.g., obvious favoring of contralateral limb and/or reduced use of entire limb; 3 =

390   complete limb paralysis) for each of the four limbs. Other detailed observations were

391   recorded based on a standard lexicon. Body weights were also collected at baseline, day

392   0, and 1, 3, 5, 7, 10, 14, and 26 days post-infection.

393

394   *Blood Collection*

395   Blood was collected at baseline and 26 days post-infection for detection of serum anti-

396   EV-D68 antibodies by western blot. Blood was collected from the femoral, saphenous or

397   cephalic veins, and was performed in sedated or anesthetized animals. Whole blood was

398   collected into serum separator tubes (SST) at each scheduled timepoint. Blood collected

399   into SST was centrifuged at 2500 x *g* for 10 minutes at room temperature for isolation of

400   serum. Sample aliquots were stored at -70ºC or below until analysis.

401

402   *Nasal Swab Collection*

403   Nasal swabs were collected for measurement of viral burden at baseline and 1, 3, 5, 7,

404   10, 14, and 26 days post-infection. Samples were collected from sedated or anesthetized

405   animals. Nylon flocked swabs (FLOQSwab, COPAN Diagnostics, Inc.) were advanced

406   into the nasal cavity, and both nostrils were sampled using a single swab. Two swabs

407   were collected per site. One swab was placed in a tube containing approximately 0.5 mL

408   sterile saline and immediately frozen on dry ice prior to storage at -70 to -90ºC. The

409   second swab was placed in a tube containing 1 mL of Trizol, was allowed to set at room

410   temperature for 15 minutes, and then frozen on dry ice prior to storage at -70 to -90ºC.

411

412

413

414 *Bronchoalveolar Lavage Fluid Collection*

415 At baseline and 3, 7, 14, and 26 days post-infection, bronchoalveolar lavage fluid (BALF)

416 was collected for quantification of viral load. BALF was collected using a pediatric

417 bronchoscope (Olympus XP40) that was advanced approximately 3-4 generations into

418 the airways of one side of the lung. Approximately 5 mL sterile saline was instilled and

419 then aspirated. The site of sample collection alternated between the left and right lung at

420 each sequential timepoint. The total recovered volume was recorded. Samples were

421 stored on wet ice until processing, at which time they were centrifuged at approximately

422 1000 x *g* at 4°C for 10 minutes. The supernatants were aliquoted and stored at -70°C or

423 below until analysis. The cell pellets were resuspended in media, and total cell counts

424 and cell differentials were performed on stained cytospins. The remaining dry cell pellet

425 was stored at -70°C.

426

427 *Cerebrospinal Fluid Collection*

428 At baseline, 3, 7, 14, and 26 days post-infection, cerebrospinal fluid (CSF) was collected

429 for quantification of viral load. Animals were anesthetized with ketamine and xylazine for

430 collections. The back of the head was clipped and sterile prepped. Approximately 0.3 mL

431 CSF was collected by sterile puncture of the cisterna magna using a 22 G, 1" needle.

432 CSF was stored in two aliquots at -70°C or below until analysis.

433

434 *Necropsy and Tissue Collection*

435 At 26-28 days post-infection, animals were euthanized for terminal tissue collections.

436 Terminal heart and lung weights were obtained and normalized to terminal body weights

437   and brain weight, and ratios were calculated for each animal. Sections of the right lung

438   were collected and flash frozen in liquid nitrogen for viral quantification assays (i.e., RT-

439   qPCR and $TCID_{50}$). All frozen samples were stored at -70 °C or below until processing

440   and analysis. The thoracic trachea, left lungs and tracheobronchial lymph nodes were

441   fixed in 10% neutral buffered formalin (NBF) and then processed for microscopic

442   examination. The left lung was inflated with 10% NBF to a fixed hydrostatic pressure of

443   25 cm. After fixation, tissues were trimmed and paraffin embedded for histopathology.

444   The brain and spinal cord were dissected, and sections were reserved for both viral

445   quantification assays (i.e., RT-qPCR and $TCID_{50}$) and histopathology. Samples for RT-

446   qPCR and $TCID_{50}$ were stored at -70 °C or below until processing and analysis. Samples

447   for histopathology were fixed in 10% NBF until trimming, paraffin embedding, sectioning,

448   and staining.

449

450   *Histopathology*

451   Formalin-fixed, paraffin-embedded tissues were sectioned and mounted on glass slides.

452   Slides were deparaffinized with xylene and rehydrated with ethyl alcohol and water for

453   staining with hematoxylin and eosin using a Tissue-Tek Automatic Slide Stainer.

454   Microscopic examination was performed by a board-certified veterinary pathologist, and

455   histologic lesions were scored based on the severity and distribution of pathology.

456   Histopathologic changes in the examined tissues were graded semi-quantitatively by a

457   single pathologist on a scale of 0-5. Histopathology was not performed blinded.

458

459

460 *Reverse-Transcription PCR (RT-PCR)*

461 Nasal swabs, CSF, and BALF supernatants were stored at -70 to -90°C until the end of

462 the study, at which time a subset of samples was designated for quantification of EV-D68

463 genome copies by RT-qPCR. Samples were centrifuged at 4000 x *g* for 5 minutes, and

464 supernatants were harvested. RNA was isolated using the QIAGEN RNeasy Kit or

465 equivalent, according to the manufacturer's instructions.

466 EV-D68 genome copies were quantified from extracted RNA samples by RT-qPCR.

467 Genome copies per mL or swab equivalents were calculated from a standard curve

468 generated from RNA standards of known copy concentration. All samples were analyzed

469 in triplicate.

470 The EV-D68 primers and probe sequences were as follows:

471 EV-D68 Forward: 5' CATGAGGCAGTAGCCATTGA 3'
472 EV-D68 Reverse: 5' CTGTACTCTCGGTTTCCCATTT 3'
473 EV-D68 Probe: 6FAM-AACCCACACAACCAGAAACCGCTA-BHQ-1

474 Amplification and detection was performed using a suitable real-time thermal cycler under

475 the following cycling conditions: 50 °C for 5 minutes, 95 °C for 20 seconds and 40 cycles

476 of 95 °C for 3 seconds, and 60 °C for 30 seconds.

477

478 *Median Tissue Culture Infectious Dose (TCID$_{50}$) Assay*

479 Nasal swabs, CSF, BALF supernatants, and terminal tissue samples were shipped to the

480 Pekosz laboratory at Johns Hopkins for processing and determination of infectious viral

481 loads by TCID$_{50}$ assay. In brief, RD cells were plated in 96-well plates, grown to full

482 confluence, and washed with PBS+. Tenfold serial dilutions of the virus inoculum were

483 made, and 200 μL of dilution was added to each of 6 wells in the plate, followed by

484   incubation at 32°C for 5-7 days. Cells were fixed by adding 100 µL of 4% formaldehyde

485   in PBS per well and incubated at room temperature for at least 10 minutes before staining

486   with Naphthol Blue Black solution. $TCID_{50}$ calculations were determined by the Reed-

487   Muench method.

488

489   *Western Blot*

490   The antibodies against structural proteins of EV-D68 were detected in a Western blot

491   assay. HeLa cells were infected with a multiplicity of infection (MOI) of 10 of either a

492   Newcastle Disease virus vector co-expressing the precursor of capsid protein P1 and

493   protease 3CD of the EV-D68 (Fermon), or a control vector expressing EGFP and RFP

494   instead of EV-D68 proteins, as previously described (Viktorova et al., 2018). The cells

495   were lysed at 24 hours post-infection, and the lysates were resolved on a 12% or 4-15%

496   gradient PAGE and transferred to a PVDF membrane to generate multiple membrane

497   strips with both lysates located side by side. The 1:1000 dilutions of pre- and post-

498   immunization sera samples from the same animal were incubated with separate

499   membrane strips each containing an EV-D68-positive and a control lane for one hour.

500   After the primary antibody incubation, the membranes were incubated with the goat anti-

501   monkey IgG secondary antibodies conjugated to horseradish peroxidase (ThermoFisher)

502   and developed with Amersham ECL Select chemiluminescent detection reagent (VWR)

503   according to the manufacturers' protocols. The signal was recorded with an Azure

504   Biosystems C500 digital luminescence detection system. The signals unique to the post-

505   immune sera in the membrane lane containing EV-D68 proteins were considered positive

506   for anti-EV-D68 antibody response.

507   *Data Analysis*

508   All graphical presentations and statistical analyses were performed using GraphPad

509   Prism software. For RT-qPCR and $TCID_{50}$ assays, samples that were below the lower

510   limit of quantification (LLOQ) for the assay were assigned a value equal to half the LLOQ.

511   Due to the low sample size in each experimental group, no formal statistical analyses

512   were performed as part of this study.

513

514

515   **Acknowledgements**

516   This project was funded in part with Federal funds from the National Institute of Allergy

517   and Infectious Diseases, National Institutes of Health, Department of Health and Human

518   Services, under Contract No. HHSN272201700024I/75N93020F00001/B07. The

519   schematic presented in Figure 1 was prepared using BioRender.com.

520

521   **Author Contributions**

522   MSV and AP conceptualized and designed the EV-D68 infection studies. AP and AC

523   propagated and titrated all EV-D68 stocks for animal infections. JD and MSV performed

524   all animal studies. CB and AR performed all RT-qPCR analyses. SMB performed all

525   histopathology. AC and ML performed all $TCID_{50}$ assays. GAB and AZ performed all

526   western blot analyses. JD, DRA and MSV performed all data compilation, analysis and

527   interpretation. All authors participated in the writing of the manuscript and approved the

528   final version.

Figure 1
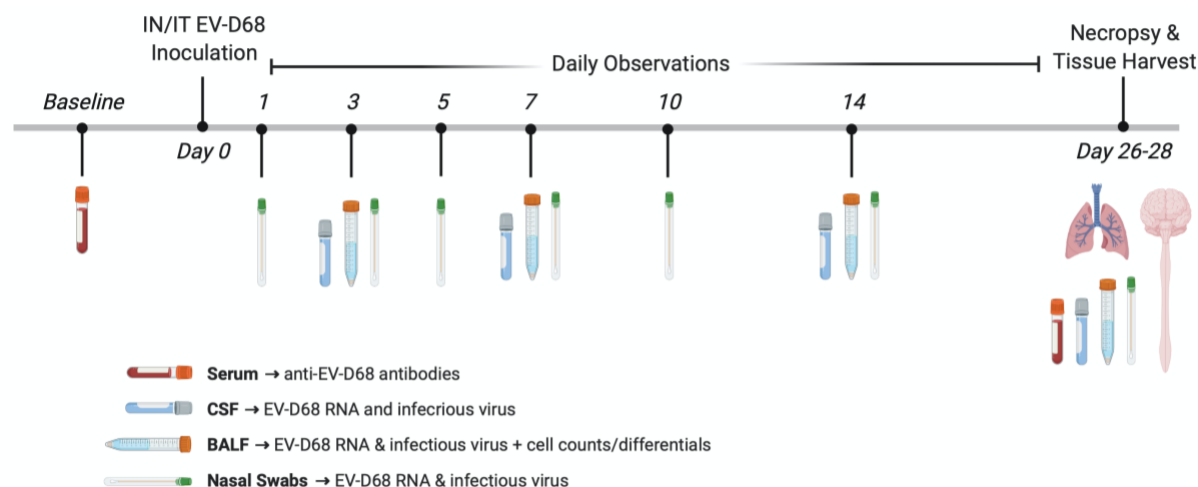
Figure 1. Experimental design and timeline. On study day 0, juvenile NHPs were inoculated with one of five different EV-D68 isolates by the respiratory route (n=2-3 per NHP species per EV-D68 isolate). Animals were monitored daily for evidence of clinical disease. Nasal swabs were collected 1, 3, 5, 7, 10, 14 and 26-28 days post-infection (dpi). Bronchoalveolar lavage fluid (BALF) and cerebrospinal fluid (CSF) were collected 3, 7, 14 and 26-28 dpi. EV-D68 RNA and infectious virus was quantified from nasal swabs, BALF and CSF by reverse-transcriptase quantitative PCR (RT-qPCR) and median tissue culture infectious dose ($TCID_{50}$) assay, respectively. Cell counts and differentials were quantified from BALF cell pellets. Anti-EV-D68 antibodies were measured in serum collected at baseline and 26 dpi. Terminally collected respiratory tract and central nervous system tissues were formalin fixed and evaluated by histopathology.

Figure 2

a

Gastrointestinal Disease Incidence

	0	1	2	3	4	5	6	7	8	9	10	11	12	13	14
PTM - IL/14	0	0	0	0	0	0	0	0	50	50	50	50	50	50	50
Cyno - IL/14	0	0	0	0	0	0	0	0	50	50	100	0	100	50	0
AGM - IL/14	0	0	0	0	0	0	0	0	0	0	0	0	0	0	0
PTM - MO/14	0	0	0	0	0	0	0	0	50	50	50	50	50	50	50
Cyno - MO/14	0	0	0	0	0	0	0	0	0	100	100	100	50	50	0
AGM - MO/14	0	0	0	0	0	0	0	0	0	0	0	0	0	0	0
Cyno - MD/18	50	50	0	50	50	100	100	100	50	0	50	100	50	50	100
RM - MD/18	0	0	0	0	0	0	0	0	0	0	0	33	0	0	0
Cyno - MN/18	50	0	0	0	100	100	100	100	50	0	50	100	50	0	0
RM - MN/18	0	0	0	0	0	0	0	0	0	0	50	0	0	0	0
RM - WA/18	0	0	0	0	0	0	0	0	0	0	0	0	0	0	0

days post-infection

b

Respiratory Disease Incidence

	0	1	2	3	4	5	6	7	8	9	10	11	12	13	14
PTM - IL/14	0	0	0	0	0	0	0	0	0	50	50	0	50	0	100
Cyno - IL/14	0	0	0	0	0	0	0	0	0	0	0	0	0	0	0
AGM - IL/14	0	50	0	0	0	0	0	0	0	0	0	0	0	0	50
PTM - MO/14	0	0	0	0	0	0	0	0	0	0	50	0	0	0	0
Cyno - MO/14	0	0	0	0	0	0	0	0	0	0	50	0	0	0	0
AGM - MO/14	0	0	0	0	0	0	0	0	0	50	50	0	50	0	0
Cyno - MD/18	0	0	0	0	0	0	0	0	0	0	0	0	0	0	0
RM - MD/18	0	0	0	0	0	0	0	0	0	0	0	0	0	0	0
Cyno - MN/18	0	0	0	0	0	0	0	0	0	0	0	0	0	0	0
RM - MN/18	0	0	0	0	0	0	0	0	0	0	0	0	0	0	0
RM - WA/18	0	0	0	0	0	0	0	0	0	0	0	0	0	0	0

days post-infection

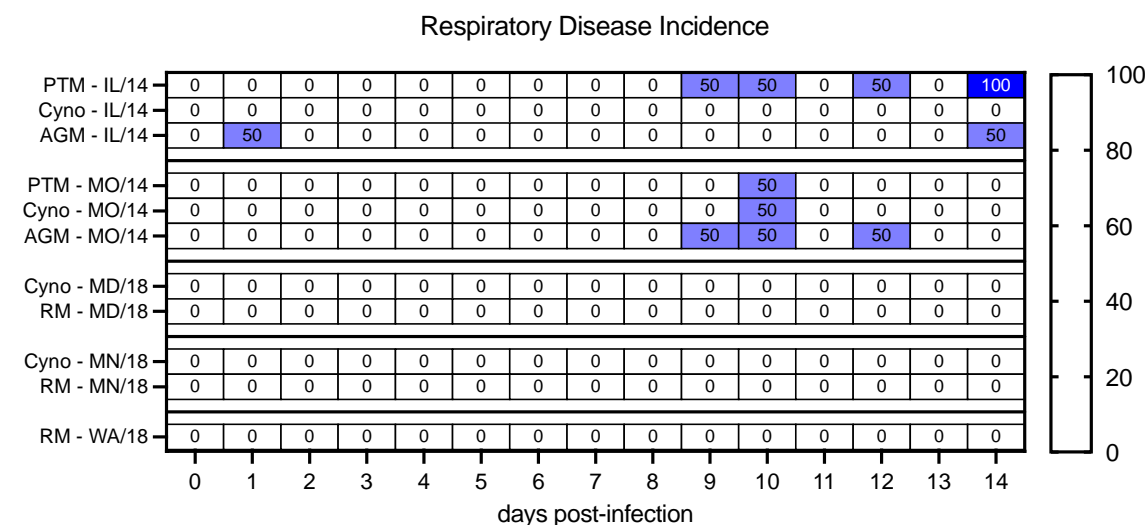**Figure 2. Clinical disease following EV-D68 infection of juvenile NHPs was mild and sporadic.** Juvenile NHPs were inoculated with one of five different EV-D68 isolates by the respiratory route (n=2-3 per NHP species per EV-D68 isolate). Animals were monitored daily for evidence of clinical disease, and observations were categorized as either **a)** gastrointestinal (e.g., diarrhea or soft stool) or **b)** respiratory (e.g., nasal or ocular discharge). There were no observations associated with acute flaccid myelitis or other neurologic disease (e.g., paresis or paralysis). The incidence of each observation within each experimental group was calculated as a percentage for each observation day. PTM = pigtailed macaque; Cyno = cynomolgus macaque; AGM = African green monkey; RM = rhesus macaque.

Figure 3

a

b

c

d
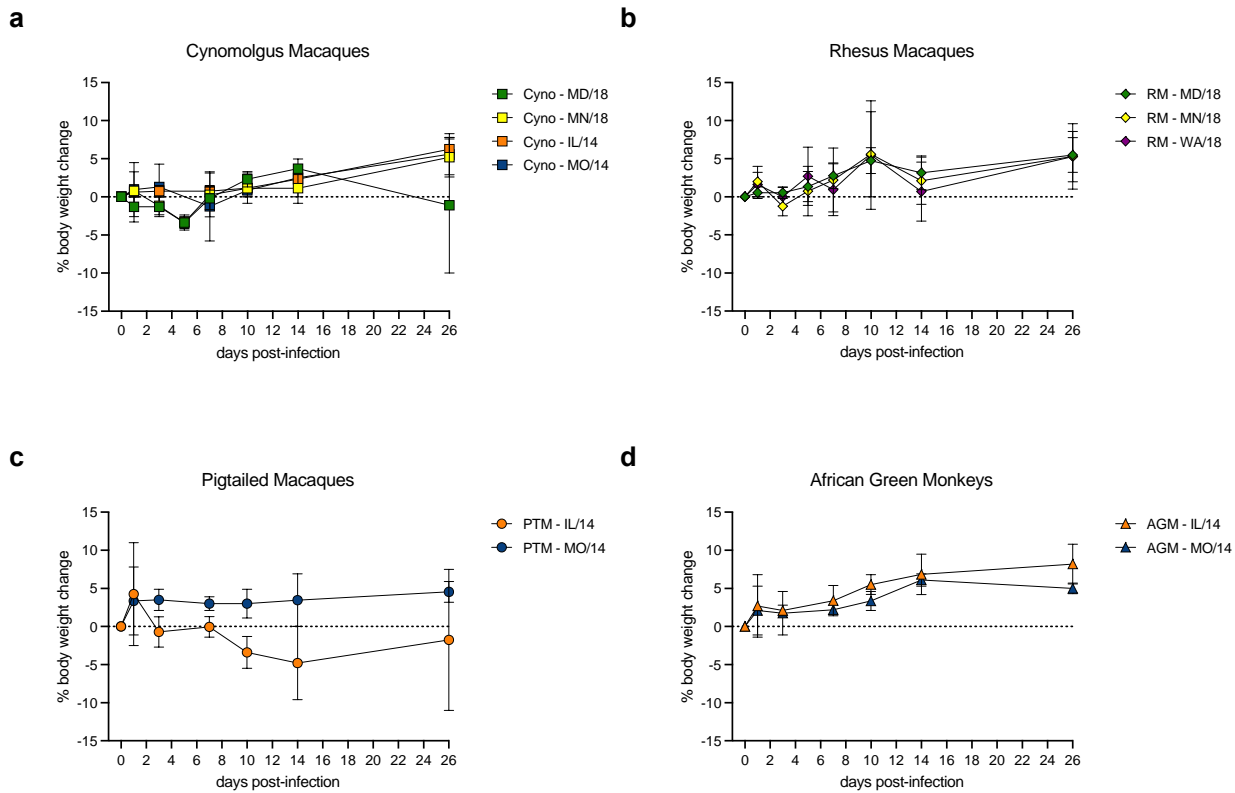
Figure 3. EV-D68 infection of juvenile NHPs resulted in minimal or no weight loss.
Juvenile cynomolgus macaques (**a**), rhesus macaques (**b**), pigtailed macaques (**c**), and
African green monkeys (**d**) were inoculated with one of five different EV-D68 isolates by
the respiratory route (n=2-3 per NHP species per EV-D68 isolate). Body weights were
collected concurrent with anesthetized procedures up to 26 days post-infection. The
percent body weight change from baseline was calculated for each animal, and the mean
+/- the standard error are shown for each group. PTM = pigtailed macaque; Cyno =
cynomolgus macaque; AGM = African green monkey; RM = rhesus macaque.

Figure 4

a

b

c

d
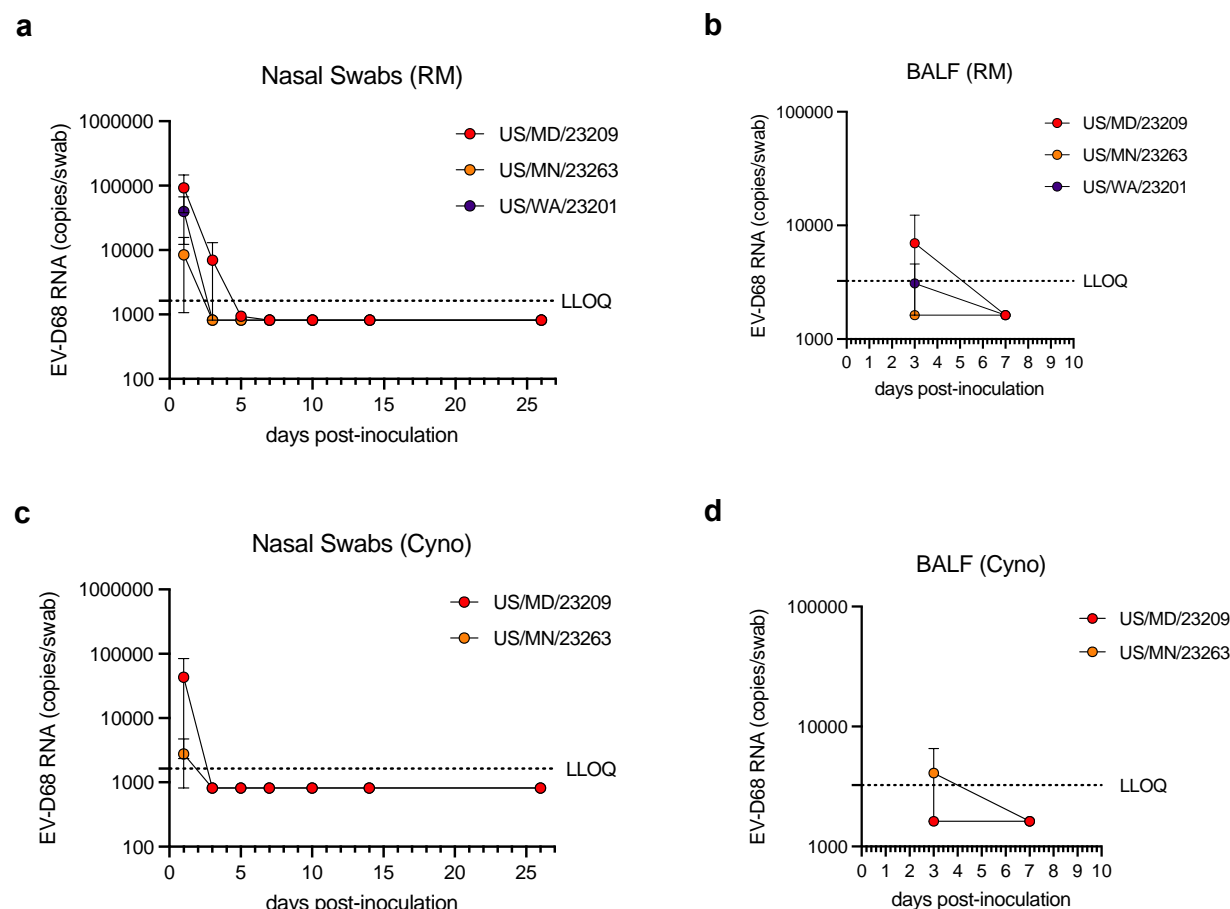
**Figure 4. EV-D68 2018 infection resulted in limited and transient detection of viral RNA in the upper and lower respiratory tract.** Juvenile rhesus and cynomolgus macaques were inoculated with one of three different 2018 EV-D68 isolates by the respiratory route (n=2-3 per NHP species per EV-D68 isolate). Nasal swabs (**a** and **c**) and bronchoalveolar lavage fluid (BALF, **b** and **d**) were serially collected from each animal up to 26 days post-infection (dpi), and EV-D68 RNA was quantified by RT-qPCR. RNA copies per swab or copies per mL were calculated for each sample, and the mean +/- the standard error are shown for each group. Cyno = cynomolgus macaque; RM = rhesus macaque. LLOQ = lower limit of quantification.

Figure 5
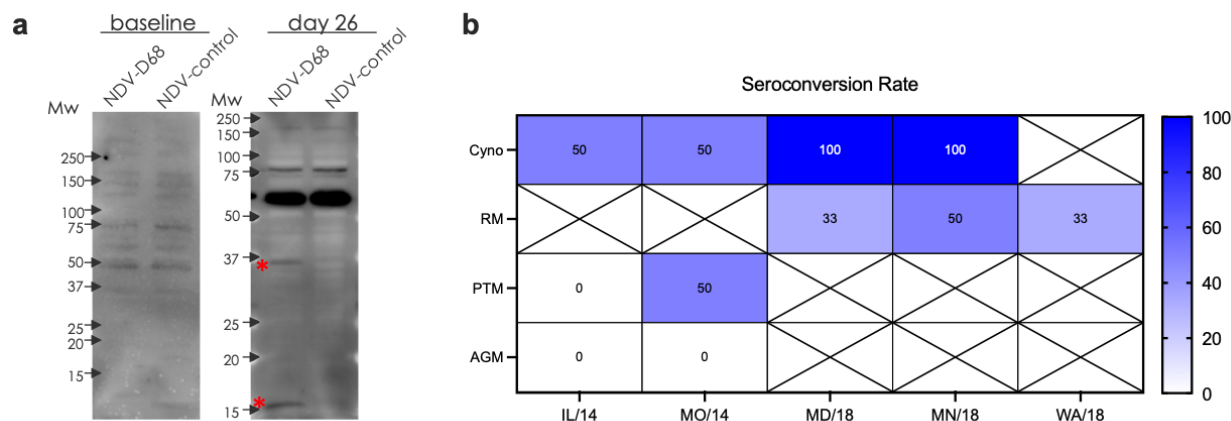
Figure 5. Anti-EV-D68 antibodies were detectable in the serum of juvenile NHPs following respiratory challenge with contemporary EV-D68 isolates. Juvenile cynomolgus macaques, rhesus macaques, pigtailed macaques, and African green monkeys were inoculated with one of five different EV-D68 isolates by the respiratory route (n=2-3 per NHP species per EV-D68 isolate). Blood was collected at baseline and at 26 days post-infection (dpi) for detection of serum antibodies against the EV-D68 structural proteins by western blot assay. A representative western blot shows positive bands at ~35 and ~15 kDa (asterisks), which represent antibodies against EV-D68 capsid proteins at 26 dpi (**a**). The seroconversion rate was calculated as a percentage for each experimental group (**b**). PTM = pigtailed macaque; Cyno = cynomolgus macaque; AGM = African green monkey; RM = rhesus macaque.

Figure 6

a

b

c

d
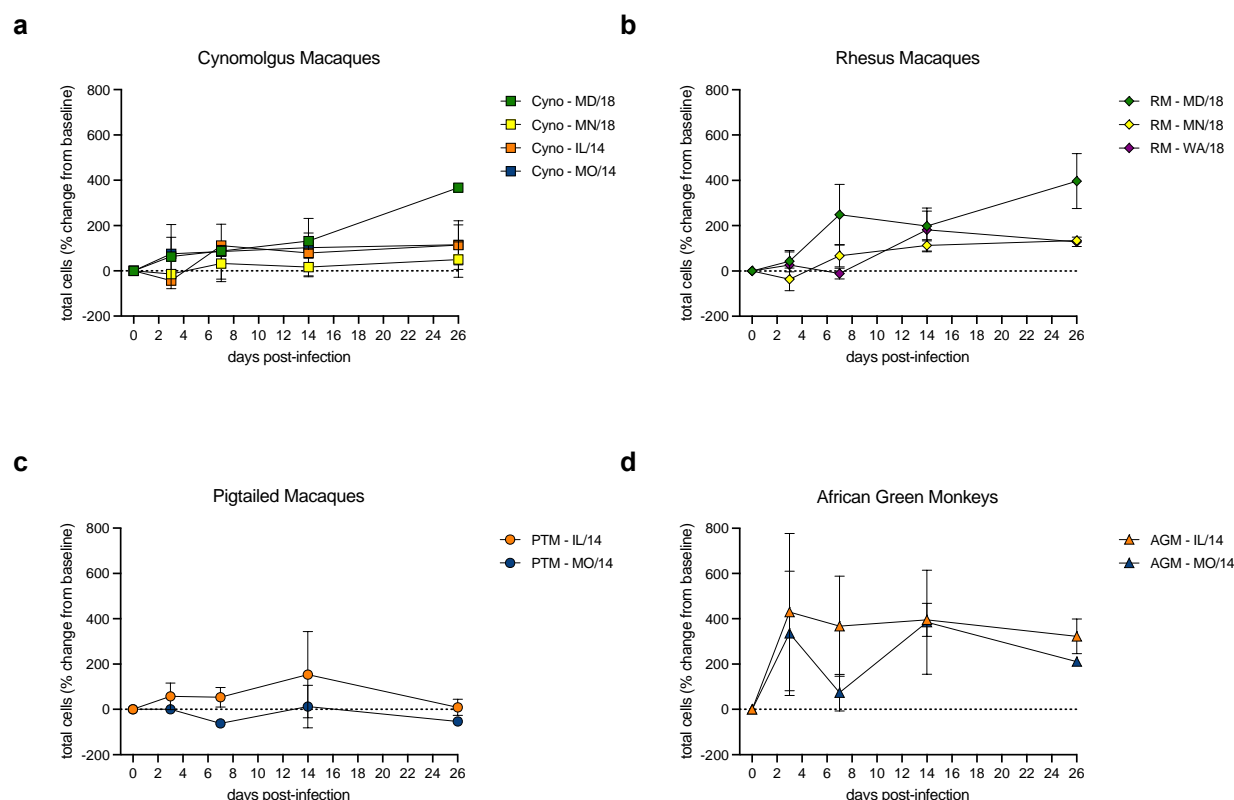
Figure 6. Airway inflammation following EV-D68 infection of juvenile NHPs was species and strain specific. Juvenile cynomolgus macaques (**a**), rhesus macaques (**b**), pigtailed macaques (**c**), and African green monkeys (**d**) were inoculated with one of five different EV-D68 isolates by the respiratory route (n=2-3 per NHP species per EV-D68 isolate). Bronchoalveolar lavage fluid (BALF) was serially collected from each animal up to 26 days post-infection (dpi), and total live cells were quantified from BALF cytospins. The percent change from baseline in total cells was calculated for each sample, and the mean +/- the standard error are shown for each group. PTM = pigtailed macaque; Cyno = cynomolgus macaque; AGM = African green monkey; RM = rhesus macaque.

604 **Table 1.** Animal Information and Group Assignments

Lovelace Study Protocol	Group	Study Cohort	Animal ID	Study ID	Age at Study Start (mos)	Weight at Study Start (kg)	Sex (M/F)	NHP Species	EV-D68 Isolate	Infection Titer ($TCID_{50}$)
FY21-131A	1	1	Z20076	1001	10.1	1.68	F	PTM	US-IL/14-18152	4×10^7
FY21-131A	1	2	Z20079	1002	10.1	1.68	M	PTM	US-IL/14-18152	4×10^7
FY21-131A	2	1	20-134	2001	8.2	1.28	F	Cyno	US-IL/14-18152	4×10^7
FY21-131A	2	2	20-099	2002	9.3	1.34	F	Cyno	US-IL/14-18152	4×10^7
FY21-131A	3	1	20-260	3001	8.4	1.44	F	AGM	US-IL/14-18152	4×10^7
FY21-131A	3	2	20-155	3002	8.8	1.52	M	AGM	US-IL/14-18152	4×10^7
FY21-131A	4	1	Z20053	4001	10.4	2.00	F	PTM	US/MO/14-18947	4×10^7
FY21-131A	4	2	Z20089	4002	9.2	2.00	M	PTM	US/MO/14-18947	4×10^7
FY21-131A	5	1	20-090	5001	9.3	1.40	M	Cyno	US/MO/14-18947	4×10^7
FY21-131A	5	2	20-121	5002	8.6	1.26	F	Cyno	US/MO/14-18947	4×10^7
FY21-131A	6	1	20-264	6001	8.6	1.82	F	AGM	US/MO/14-18947	4×10^7
FY21-131A	6	2	20-157	6002	10.0	1.94	M	AGM	US/MO/14-18947	4×10^7
FY21-131B	1	1	20-413	1001	10.4	1.54	M	Cyno	US/MD/18-23209	4×10^6
FY21-131B	1	2	20-519	1002	9.4	1.14	F	Cyno	US/MD/18-23209	4×10^6
FY21-131B	2	1	20C287	2001	11.4	2.42	M	RM	US/MD/18-23209	4×10^6
FY21-131B	2	2	20C286	2002	11.5	2.20	M	RM	US/MD/18-23209	4×10^6
FY21-131B	2	1	20C288	2003	10.8	1.96	F	RM	US/MD/18-23209	4×10^6
FY21-131B	3	2	20-461	3001	10.1	1.10	M	Cyno	US/MN/18-23263	4×10^6
FY21-131B	3	1	20-520	3002	9.3	1.32	F	Cyno	US/MN/18-23263	4×10^6
FY21-131B	4	1	20C280	4001	11.8	2.54	M	RM	US/MN/18-23263	4×10^6
FY21-131B	4	2	20C289	4002	10.4	1.94	F	RM	US/MN/18-23263	4×10^6
FY21-131B	5	2	20C285	5001	11.5	2.13	M	RM	US/WA/18-23201	4×10^6
FY21-131B	5	1	20C284	5002	11.7	1.96	F	RM	US/WA/18-23201	4×10^6
FY21-131B	5	2	29C283	5003	11.8	2.26	F	RM	US/WA/18-23201	4×10^6

605
606   PTM = Pigtail macaque   Cyno = Cynomolgus macaque   AGM = African green monkey
607   RM = Rhesus macaque

608 **Table 2.** Clinical Observations

Study ID	Sex (M/F)	NHP Species	EV-D68 Isolate	Study Day (relative to EV-D68 challenge)															
				0	1	2	3	4	5	6	7	8	9	10	11	12	13	14	26
1001	F	PTM	IL/14	-	-	-	-	-	-	-	-	-	-	N, R	-	-	-	N	N, A, R
1002	M	PTM	IL/14	-	-	-	-	-	-	-	-	S	C, S	S	S	N, S	S	N, S	R
2001	F	Cyno	IL/14	-	-	-	-	-	-	-	-	-	-	S	-	S	S	-	-
2002	F	Cyno	IL/14	-	-	-	-	-	-	-	-	S	S	S	-	S	-	-	N
3001	F	AGM	IL/14	-	-	-	-	-	-	-	-	-	-	-	-	-	-	-	-
3002	M	AGM	IL/14	-	N	-	-	-	-	-	-	-	-	-	-	-	-	N	-
4001	F	PTM	MO/14	-	-	-	-	-	-	-	-	-	-	N	-	-	-	-	-
4002	M	PTM	MO/14	-	-	-	-	-	-	-	-	S	S	S	S	S	S	S	-
5001	M	Cyno	MO/14	-	-	-	-	-	-	-	-	-	S	S	S	-	S	-	-
5002	F	Cyno	MO/14	-	-	-	-	-	-	-	-	-	S	N, S	S	S	-	-	-
6001	F	AGM	MO/14	-	-	-	-	-	-	-	-	-	-	O	-	-	-	-	-
6002	M	AGM	MO/14	-	-	-	-	-	-	-	-	-	N	-	-	N	-	-	-
1001	M	Cyno	MD/18	S	-	-	-	-	S	S	S	S	-	-	S	S	-	S	-
1002	F	Cyno	MD/18	-	S	-	S	S	S	S	S	-	-	S	S	-	S	S	A, R
2001	M	RM	MD/18	-	-	-	-	-	-	-	-	-	-	-	-	-	-	-	-
2002	M	RM	MD/18	-	-	-	-	-	-	-	-	-	-	-	-	-	-	-	-
2003	F	RM	MD/18	-	-	-	-	-	-	-	-	-	-	-	S	-	-	-	-
3001	M	Cyno	MN/18	-	-	-	-	S	S	S	S	-	-	S	S	-	-	-	-
3002	F	Cyno	MN/18	S	-	-	-	S	S	S	S	S	-	-	S	S	-	-	-
4001	M	RM	MN/18	-	-	-	-	-	-	-	-	-	-	-	-	-	-	-	-
4002	F	RM	MN/18	-	-	-	-	-	-	-	-	-	-	S	-	-	-	-	-
5001	M	RM	WA/18	-	-	-	-	-	-	-	-	-	-	-	-	-	-	-	-
5002	F	RM	WA/18	-	-	-	-	-	-	-	-	-	-	-	-	-	-	-	-
5003	F	RM	WA/18	-	-	-	-	-	-	-	-	-	-	-	-	-	-	-	-

609
610   PTM = Pigtail macaque   Cyno = Cynomolgus macaque   AGM = African green monkey
611   RM = Rhesus macaque   IL = US-IL/14-18152   MO = US/MO/14-18947
612   MD = US/MD/18-23209   MN = US/MN/18-23263   WA = US/WA/18-23201
613   N = nasal discharge   O = ocular discharge   S = soft stool/diarrhea
614   C = cough   R = reduced activity   A = abnormal posture

615 **Table 3.** EV-D68 RNA Concentrations and Western Blot Results

Animal ID	Sex (M/F)	NHP Species	EV-D68 Isolate	EV-D68 RNA (copies/swab or copies/mL)							Western Blot Results
				Nasal Swabs				BALF		CSF	
				1 dpi	3 dpi	5 dpi	7 dpi	3 dpi	7 dpi	3 dpi	
1001	F	PTM	IL	BQL	BQL	BQL	BQL	BQL	BQL	BQL	NEG
1002	M	PTM	IL	BQL	BQL	BQL	BQL	BQL	BQL	BQL	NEG
2001	F	Cyno	IL	BQL	BQL	BQL	BQL	BQL	BQL	BQL	POS
2002	F	Cyno	IL	BQL	BQL	BQL	BQL	BQL	BQL	BQL	NEG
3001	F	AGM	IL	BQL	BQL	BQL	BQL	BQL	BQL	BQL	NEG
3002	M	AGM	IL	BQL	BQL	BQL	BQL	BQL	BQL	BQL	NEG
4001	F	PTM	MO	BQL	BQL	BQL	BQL	BQL	BQL	BQL	POS
4002	M	PTM	MO	BQL	BQL	BQL	BQL	BQL	BQL	BQL	NEG
5001	M	Cyno	MO	BQL	BQL	BQL	BQL	BQL	BQL	BQL	POS
5002	F	Cyno	MO	BQL	BQL	BQL	BQL	BQL	BQL	BQL	NEG
6001	F	AGM	MO	BQL	BQL	BQL	BQL	BQL	BQL	BQL	NEG
6002	M	AGM	MO	BQL	BQL	BQL	BQL	BQL	BQL	BQL	NEG
1001	M	Cyno	MD	8.40E+04	BQL	BQL	BQL	BQL	BQL	BQL	POS
1002	F	Cyno	MD	2.35E+03	BQL	BQL	BQL	BQL	BQL	BQL	POS
2001	M	RM	MD	8.71E+04	BQL	BQL	BQL	BQL	BQL	BQL	NEG
2002	M	RM	MD	1.89E+05	1.92E+04	1.17E+03	BQL	BQL	BQL	BQL	NEG
2003	F	RM	MD	8.58E+02	BQL	BQL	BQL	1.77E+04	BQL	BQL	POS
3001	M	Cyno	MN	4.72E+03	BQL	BQL	BQL	6.58E+03	BQL	BQL	POS
3002	F	Cyno	MN	BQL	BQL	BQL	BQL	BQL	BQL	BQL	POS
4001	M	RM	MN	1.07E+03	BQL	BQL	BQL	BQL	BQL	BQL	POS
4002	F	RM	MN	1.57E+04	BQL	BQL	BQL	BQL	BQL	BQL	NEG
5001	M	RM	WA	9.23E+04	BQL	BQL	BQL	6.05E+03	BQL	BQL	POS
5002	F	RM	WA	BQL	BQL	BQL	BQL	BQL	BQL	BQL	NEG
5003	F	RM	WA	2.55E+04	BQL	BQL	BQL	BQL	BQL	BQL	NEG

616
617   PTM = Pigtail macaque   Cyno = Cynomolgus macaque   AGM = African green monkey
618   RM = Rhesus macaque   IL = US-IL/14-18152   MO = US/MO/14-18947
619   MD = US/MD/18-23209   MN = US/MN/18-23263   WA = US/WA/18-23201
620   DPI = days post-infection   BQL = below the quantification limit of the assay

621 **Table 4.** Terminal Lung Weight Ratios

Animal ID	Sex (M/F)	NHP Species	EV-D68 Isolate	Terminal Body Weight (kg)	Terminal Lung Weight (g)	Terminal Brain Weight (g)	Terminal Lung/Body Weight Ratio (g/kg)	Terminal Lung/Brain Weight Ratio (g/g)
1001	F	PTM	IL	1.72	15.43	92.06	8.973	0.168
1002	M	PTM	IL	1.74	11.71	81.34	6.729	0.144
2001	F	Cyno	IL	1.28	9.94	61.14	7.762	0.163
2002	F	Cyno	IL	1.44	10.62	62.15	7.376	0.171
3001	F	AGM	IL	1.52	11.24	61.59	7.393	0.182
3002	M	AGM	IL	1.64	11.99	62.66	7.309	0.191
4001	F	PTM	MO	1.94	12.12	79.45	6.245	0.152
4002	M	PTM	MO	2.06	14.69	90.35	7.132	0.163
5001	M	Cyno	MO	1.42	9.97	73.10	7.018	0.136
5002	F	Cyno	MO	1.30	9.55	62.12	7.347	0.154
6001	F	AGM	MO	1.84	12.42	60.60	6.751	0.205
6002	M	AGM	MO	1.96	13.04	65.94	6.652	0.198
1001	M	Cyno	MD	1.66	13.88	66.94	8.364	0.207
1002	F	Cyno	MD	1.08	7.70	54.60	7.132	0.141
2001	M	RM	MD	2.50	17.79	89.41	7.114	0.199
2002	M	RM	MD	2.28	16.23	88.42	7.119	0.184
2003	F	RM	MD	2.14	13.85	70.38	6.471	0.197
3001	M	Cyno	MN	1.18	7.39	58.32	6.263	0.127
3002	F	Cyno	MN	1.38	9.10	54.00	6.596	0.169
4001	M	RM	MN	2.74	16.70	89.73	6.095	0.186
4002	F	RM	MN	2.02	12.97	64.41	6.419	0.201
5001	M	RM	WA	2.26	15.17	84.12	6.714	0.180
5002	F	RM	WA	2.08	14.67	70.02	7.051	0.209
5003	F	RM	WA	2.38	16.00	75.25	6.723	0.213

622
623   PTM = Pigtail macaque   Cyno = Cynomolgus macaque   AGM = African green monkey
624   RM = Rhesus macaque   IL = US-IL/14-18152   MO = US/MO/14-18947
625   MD = US/MD/18-23209   MN = US/MN/18-23263   WA = US/WA/18-23201

References

Baggen, J., Thibaut, H. J., Staring, J., Jae, L. T., Liu, Y., Guo, H., Slager, J. J., de Bruin, J. W., van Vliet, A. L., Blomen, V. A., Overduin, P., Sheng, J., de Haan, C. A., de Vries, E., Meijer, A., Rossmann, M. G., Brummelkamp, T. R., & van Kuppeveld, F. J. (2016). Enterovirus D68 receptor requirements unveiled by haploid genetics. *Proc Natl Acad Sci U S A*, *113*(5), 1399-1404. https://doi.org/10.1073/pnas.1524498113

Chong, P. F., Kira, R., Mori, H., Okumura, A., Torisu, H., Yasumoto, S., Shimizu, H., Fujimoto, T., Hanaoka, N., Kusunoki, S., Takahashi, T., Oishi, K., Tanaka-Taya, K., & Acute Flaccid Myelitis Collaborative Study, I. (2018). Clinical Features of Acute Flaccid Myelitis Temporally Associated With an Enterovirus D68 Outbreak: Results of a Nationwide Survey of Acute Flaccid Paralysis in Japan, August-December 2015. *Clin Infect Dis*, *66*(5), 653-664. https://doi.org/10.1093/cid/cix860

Dyda, A., Stelzer-Braid, S., Adam, D., Chughtai, A. A., & MacIntyre, C. R. (2018). The association between acute flaccid myelitis (AFM) and Enterovirus D68 (EV-D68) - what is the evidence for causation? *Euro Surveill*, *23*(3). https://doi.org/10.2807/1560-7917.ES.2018.23.3.17-00310

Evans, W. J., Hurst, B. L., Peterson, C. J., Van Wettere, A. J., Day, C. W., Smee, D. F., & Tarbet, E. B. (2019). Development of a respiratory disease model for enterovirus D68 in 4-week-old mice for evaluation of antiviral therapies. *Antiviral Res*, *162*, 61-70. https://doi.org/10.1016/j.antiviral.2018.11.012

Greninger, A. L., Naccache, S. N., Messacar, K., Clayton, A., Yu, G., Somasekar, S., Federman, S., Stryke, D., Anderson, C., Yagi, S., Messenger, S., Wadford, D., Xia, D., Watt, J. P., Van Haren, K., Dominguez, S. R., Glaser, C., Aldrovandi, G., & Chiu, C. Y. (2015). A novel outbreak enterovirus D68 strain associated with acute flaccid myelitis cases in the USA (2012-14): a retrospective cohort study. *Lancet Infect Dis*, *15*(6), 671-682. https://doi.org/10.1016/S1473-3099(15)70093-9

Haertel, A. J., Prongay, K., Gao, L., Gottlieb, D. H., & Park, B. (2018). Standard growth and diarrhea-associated growth faltering in captive infant rhesus macaques (Macaca mulatta). *Am J Primatol*, *80*(9), e22923. https://doi.org/10.1002/ajp.22923

Hixon, A. M., Clarke, P., & Tyler, K. L. (2017). Evaluating Treatment Efficacy in a Mouse Model of Enterovirus D68-Associated Paralytic Myelitis. *J Infect Dis*, *216*(10), 1245-1253. https://doi.org/10.1093/infdis/jix468

Hixon, A. M., Yu, G., Leser, J. S., Yagi, S., Clarke, P., Chiu, C. Y., & Tyler, K. L. (2017). A mouse model of paralytic myelitis caused by enterovirus D68. *PLoS Pathog*, *13*(2), e1006199. https://doi.org/10.1371/journal.ppat.1006199

Hurst, B. L., Evans, W. J., Smee, D. F., Van Wettere, A. J., & Tarbet, E. B. (2019). Evaluation of antiviral therapies in respiratory and neurological disease models of Enterovirus D68 infection in mice. *Virology*, *526*, 146-154. https://doi.org/10.1016/j.virol.2018.10.014

Imamura, T., Okamoto, M., Nakakita, S., Suzuki, A., Saito, M., Tamaki, R., Lupisan, S., Roy, C. N., Hiramatsu, H., Sugawara, K. E., Mizuta, K., Matsuzaki, Y., Suzuki, Y., & Oshitani, H. (2014). Antigenic and receptor binding properties of enterovirus 68. *J Virol*, *88*(5), 2374-2384. https://doi.org/10.1128/JVI.03070-13

Kamau, E., Harvala, H., Blomqvist, S., Nguyen, D., Horby, P., Pebody, R., & Simmonds, P. (2019). Increase in Enterovirus D68 Infections in Young Children, United Kingdom, 2006-2016. *Emerg Infect Dis*, *25*(6), 1200-1203. https://doi.org/10.3201/eid2506.181759

Knoester, M., Helfferich, J., Poelman, R., Van Leer-Buter, C., Brouwer, O. F., Niesters, H. G. M., & Group, E.-D. A. W. (2019). Twenty-nine Cases of Enterovirus-D68-associated Acute Flaccid Myelitis in Europe 2016: A Case Series and Epidemiologic Overview. *Pediatr Infect Dis J*, *38*(1), 16-21. https://doi.org/10.1097/INF.0000000000002188

676 Kuchipudi, S. V., Nelli, R. K., Gontu, A., Satyakumar, R., Surendran Nair, M., & Subbiah, M.
677   (2021). Sialic Acid Receptors: The Key to Solving the Enigma of Zoonotic Virus Spillover.
678   *Viruses*, *13*(2). https://doi.org/10.3390/v13020262
679 Lang, M., Mirand, A., Savy, N., Henquell, C., Maridet, S., Perignon, R., Labbe, A., & Peigue-
680   Lafeuille, H. (2014). Acute flaccid paralysis following enterovirus D68 associated
681   pneumonia, France, 2014. *Euro Surveill*, *19*(44). https://doi.org/10.2807/1560-
682   7917.es2014.19.44.20952
683 Liu, Y., Sheng, J., Baggen, J., Meng, G., Xiao, C., Thibaut, H. J., van Kuppeveld, F. J., &
684   Rossmann, M. G. (2015). Sialic acid-dependent cell entry of human enterovirus D68. *Nat
685   Commun*, *6*, 8865. https://doi.org/10.1038/ncomms9865
686 Messacar, K., Abzug, M. J., & Dominguez, S. R. (2016). 2014 outbreak of enterovirus D68 in
687   North America. *J Med Virol*, *88*(5), 739-745. https://doi.org/10.1002/jmv.24410
688 Miller, L. A., Royer, C. M., Pinkerton, K. E., & Schelegle, E. S. (2017). Nonhuman Primate Models
689   of Respiratory Disease: Past, Present, and Future. *ILAR J*, *58*(2), 269-280.
690   https://doi.org/10.1093/ilar/ilx030
691 Morens, D. M., Folkers, G. K., & Fauci, A. S. (2019). Acute Flaccid Myelitis: Something Old and
692   Something New. *mBio*, *10*(2). https://doi.org/10.1128/mBio.00521-19
693 Morrey, J. D., Wang, H., Hurst, B. L., Zukor, K., Siddharthan, V., Van Wettere, A. J., Sinex, D. G.,
694   & Tarbet, E. B. (2018). Causation of Acute Flaccid Paralysis by Myelitis and Myositis in
695   Enterovirus-D68 Infected Mice Deficient in Interferon alphabeta/gamma Receptor
696   Deficient Mice. *Viruses*, *10*(1). https://doi.org/10.3390/v10010033
697 Nix, W. A., Jiang, B., Maher, K., Strobert, E., & Oberste, M. S. (2008). Identification of
698   enteroviruses in naturally infected captive primates. *J Clin Microbiol*, *46*(9), 2874-2878.
699   https://doi.org/10.1128/JCM.00074-08
700 Patel, M. C., Wang, W., Pletneva, L. M., Rajagopala, S. V., Tan, Y., Hartert, T. V., Boukhvalova,
701   M. S., Vogel, S. N., Das, S. R., & Blanco, J. C. (2016). Enterovirus D-68 Infection,
702   Prophylaxis, and Vaccination in a Novel Permissive Animal Model, the Cotton Rat
703   (Sigmodon hispidus). *PLoS One*, *11*(11), e0166336.
704   https://doi.org/10.1371/journal.pone.0166336
705 Shen, L., Chen, C. Y., Huang, D., Wang, R., Zhang, M., Qian, L., Zhu, Y., Zhang, A. Z., Yang, E.,
706   Qaqish, A., Chumakov, K., Kouiavskaia, D., Vignuzzi, M., Nathanson, N., Macadam, A. J.,
707   Andino, R., Kew, O., Xu, J., & Chen, Z. W. (2017). Pathogenic Events in a Nonhuman
708   Primate Model of Oral Poliovirus Infection Leading to Paralytic Poliomyelitis. *J Virol*,
709   *91*(14). https://doi.org/10.1128/JVI.02310-16
710 Urbanski, H. F., Kohama, S. G., West, G. A., Glynn, C., Williams-Karnesky, R. L., Earl, E.,
711   Neuringer, M. N., Renner, L., Weiss, A., Stenzel-Poore, M., & Bahjat, F. R. (2012).
712   Changes in spontaneous activity assessed by accelerometry correlate with extent of
713   cerebral ischemia-reperfusion injury in the nonhuman primate. *Transl Stroke Res*, *3*(4),
714   442-451. https://doi.org/10.1007/s12975-012-0191-8
715 Vermillion, M. S., Murakami, E., Ma, B., Pitts, J., Tomkinson, A., Rautiola, D., Babusis, D., Irshad,
716   H., Siegel, D., Kim, C., Zhao, X., Niu, C., Yang, J., Gigliotti, A., Kadrichu, N., Bilello, J. P.,
717   Ellis, S., Bannister, R., Subramanian, R., . . . Porter, D. P. (2021). Inhaled remdesivir
718   reduces viral burden in a nonhuman primate model of SARS-CoV-2 infection. *Sci Transl
719   Med*, eabl828. https://doi.org/10.1126/scitranslmed.abl8282
720 Viktorova, E. G., Khattar, S. K., Kouiavskaia, D., Laassri, M., Zagorodnyaya, T., Dragunsky, E.,
721   Samal, S., Chumakov, K., & Belov, G. A. (2018). Newcastle Disease Virus-Based
722   Vectored Vaccine against Poliomyelitis. *Journal of Virology*, *92*(17). https://doi.org/ARTN
723   e00976-18
724 10.1128/JVI.00976-18
725 Vogt, M. R., Fu, J., Kose, N., Williamson, L. E., Bombardi, R., Setliff, I., Georgiev, I. S., Klose, T.,
726   Rossmann, M. G., Bochkov, Y. A., Gern, J. E., Kuhn, R. J., & Crowe, J. E., Jr. (2020).

727   Human antibodies neutralize enterovirus D68 and protect against infection and paralytic
728   disease. *Sci Immunol*, *5*(49). https://doi.org/10.1126/sciimmunol.aba4902
729 Zhang, C., Zhang, X., Dai, W., Liu, Q., Xiong, P., Wang, S., Geng, L., Gong, S., & Huang, Z.
730   (2018). A Mouse Model of Enterovirus D68 Infection for Assessment of the Efficacy of
731   Inactivated Vaccine. *Viruses*, *10*(2). https://doi.org/10.3390/v10020058
732 Zhang, C., Zhang, X., Zhang, W., Dai, W., Xie, J., Ye, L., Wang, H., Chen, H., Liu, Q., Gong, S.,
733   Geng, L., & Huang, Z. (2018). Enterovirus D68 virus-like particles expressed in Pichia
734   pastoris potently induce neutralizing antibody responses and confer protection against
735   lethal viral infection in mice. *Emerg Microbes Infect*, *7*(1), 3.
736   https://doi.org/10.1038/s41426-017-0005-x
737 Zheng, H., Wang, J., Li, B., Guo, L., Li, H., Song, J., Yang, Z., Li, H., Fan, H., Huang, X., Long,
738   H., Cheng, C., Chu, M., He, Z., Yu, W., Li, J., Gao, Y., Ning, R., Li, N., . . . Liu, L. (2018).
739   A Novel Neutralizing Antibody Specific to the DE Loop of VP1 Can Inhibit EV-D68 Infection
740   in Mice. *J Immunol*, *201*(9), 2557-2569. https://doi.org/10.4049/jimmunol.1800655
741 Zheng, H., Yang, Z., Li, B., Li, H., Guo, L., Song, J., Hou, D., Li, N., Yang, J., Wu, Q., Sun, M., &
742   Liu, L. (2020). Single B cells reveal the antibody responses of rhesus macaques
743   immunized with an inactivated enterovirus D68 vaccine. *Arch Virol*, *165*(8), 1777-1789.
744   https://doi.org/10.1007/s00705-020-04676-6
745 Zheng, H. W., Sun, M., Guo, L., Wang, J. J., Song, J., Li, J. Q., Li, H. Z., Ning, R. T., Yang, Z. N.,
746   Fan, H. T., He, Z. L., & Liu, L. D. (2017). Nasal Infection of Enterovirus D68 Leading to
747   Lower Respiratory Tract Pathogenesis in Ferrets (Mustela putorius furo). *Viruses*, *9*(5).
748   https://doi.org/10.3390/v9050104
749